A Comparative Study of Conceptual Model Complexity to Describe Water Flow and Nitrate Transport in Deep Unsaturated Loess

T. Turkeltaub[a], Xiaoxu Jia[b,c] , Yuanjun Zhu[c], Ming-An Shao[b,c] and Andrew Binley[a]

[a] Lancaster Environment Centre, Lancaster University, Lancaster, UK, LA1 4YQ, UK.

[b]Key Laboratory of Ecosystem Network Observation and Modeling, Institute of Geographical Sciences and Natural Resources Research, Chinese Academy of Sciences

[c] State Key Laboratory of Soil Erosion and Dryland Farming on the Loess Plateau, Northwest A&F University

Highlights

- Examination of how complex a model needs to be for the simulation of water and nitrate movement in deep unsaturated loess.
- The performance of a combined Richards' equation and Advection-Dispersion equation approach is superior to a simplistic piston flow model.
- Using a Ks decay function to represent loess vertical variability in numerical models improves unsaturated water flow predictions.

Abstract

Understanding nitrate migration through the deep vadose zone is essential for aquifer vulnerability assessments. The effect of variability of physical properties of the deep vadose zone on nitrate transport has been scarcely explored. Recently, deep nitrate storage profiles were determined in the vadose zone of the Loess Plateau of China. Using these observations along with measured soil properties, this study investigates the effect of loess vertical heterogeneity on water movement and nitrate transport through the deep vadose zone. Models of different complexity were established and calibrated. First, a simple piston flow and nitrate mass balance approach was calibrated to the observed nitrate storage. The results indicate that the total nitrate storage is estimated well, while the estimation of the distribution of nitrate is relatively poor. Subsequently, Richards' equation and the Advection-Dispersion equation were evaluated. Three different conceptualizations of the numerical models were calibrated against deep vadose zone nitrate and water content observations: (1) one-layer model assuming homogenous loess vadose zone; (2) a model that considers a hydraulic conductivity (Ks) decay function and (3) a model where the Miller-Miller scaling factors are prescribed to account for changes of the hydraulic functions with depth. Accounting for the vertical Ks decay in the numerical models improved water flow performances. The study reveals the adequacy of implementing water flow and nitrate transport numerical models together with a simple representation of the vertical loess variability, for simulating nitrate migration in loess deep vadose zone environments.

1 Introduction

The excessive use and improper management of nitrate fertilization in agricultural production have led to nitrate groundwater and surface water contamination worldwide (Kapoor & Viraraghavan, 1997; Galloway et al., 2004). It has been recognized that a substantial amount of nitrate is being stored in the deep vadose zone globally, which results in a 'time bomb' for future quality of water resources (Ascott et al., 2017). Nitrate leaching rates and nitrate migration in the vadose zone are controlled by various of factors such as fertilizer input amounts, fertilizer application frequency, water input intensity and frequency, crop type, soil texture and soil variability (Spalding & Exner, 1993; Onsoy et al., 2005; Green et al., 2008; Botros et al., 2012; Kurtzman et al., 2013; Turkeltaub et al., 2015a; Baram et al., 2016; Min et al., 2017). Understanding the dominant factors that control nitrate migration in the deep vadose zone is of great interest for water resources management.

Due to the difficultly of directly measuring contaminant fluxes in the deep vadose zone, conceptual models (of various complexity) are often used to help improve our understanding of deep vadose zone transport (e.g. Feyen et al., 1998; Baran et al., 2007; Botros et al., 2012; Russo et al., 2014; Min et al., 2015; Baram et al., 2016; Turkeltaub et al., 2015a). Generally, deep vadose zones exhibit large textural diversity and layering that can affect the flow and transport behavior (Nimmo et al., 2002; O'Geen et al., 2005; Onsoy et al., 2005). However, implementation of such layering in models is challenging, particularly as observations in the deep vadose zone are rare. Consequently, the modeler is forced to adopt a strategy employing 'effective parameters' that can capture the spatial variations of the (often limited) observed states (Mohanty & Zhu, 2007; Vereecken et al., 2007; Nasta & Romano, 2016). Effective parameters can be obtained by scaling methods, inverse modeling (calibration) or a combination of the two (Kabat et al., 1997; Zhang et al., 2004; Vereecken et al., 2007; Botros et al., 2012; Russo et al., 2014; Turkeltaub et al., 2015a,b). Generally, loess vadose zones consist of paleosol sequences which can exhibit a rather complex stratigraphy (Kukla, 1987; O'Geen et al., 2005). O'Geen et al. (2005) stated that in order to improve modeling performances for loess vadose zones, the relationships between hydrological processes and vertical variability needs to be evaluated.

The impact of soil vertical variability on unsaturated nitrate transport and other contaminants at different scales has been the focus of a number of studies (Onsoy et al., 2005; Botros et al., 2012;

Russo et al., 2014; Baram et al., 2016; Oostrom et al., 2016; Akbariyeh et al., 2018). It has been illustrated that in unconsolidated alluvial deposits under irrigated agricultural land, there are immobile regions that play a major role in defining the spatial variability of nitrate (Botros et al., 2012; Russo et al., 2014). However, under semi-arid and arid climate conditions, the heterogeneity of the deep vadose appears to have insignificant effect on contaminant flux into groundwater (Oostrom et al., 2016). The influence of soil variability on nitrate migration in the deep loess vadose zone has not been thoroughly investigated. Some studies on nitrate in the deep loess vadose zones have related the vertical variability of nitrate to processes that occurred at the loess surface, such as land use change (Baran et al., 2007; Huang et al., 2013). Other studies showed that higher recharge rates occurred at locations with homogeneous loess (O'Geen et al., 2005). Therefore, it is unclear if the migration of nitrate through the deep loess vadose zone is controlled solely by the conditions enforced at the loess surface (e.g. water input and fertilizer application), or whether other factors, such as the loess heterogeneity, play a significant role. Until such effects are evaluated, our ability to reliably model nitrate transport to deep groundwater systems is limited, with clear consequences on the validity of vulnerability assessments.

The thickest (>150 m) and largest loess deposits in the world are located in the Loess Plateau of China (LPC) (Kukla, 1987). The LPC is experiencing significant land-use change, rapid decline in the water table, climate change and intensive soil erosion processes (Zhang et al., 2008; Huang & Pang, 2011; Li et al., 2014). In addition, a number of studies that used mass balance approaches and nitrate isotope compositions analysis, indicated that nitrate is accumulating in the LPC vadose zone due to an overuse of N-based fertilizers (Huang 2013; Jia et al., 2018; Liu et al., 2019; Ji et al., 2019). Despite the immense consequences of degradation of water quality over such a large region, knowledge regarding the factors that control nitrate distribution in the vadose zone of the LPC is still limited.

Turkeltaub et al. (2018) presented the spatiotemporal patterns of vadose zone nitrate storage and groundwater in the LPC by implementing numerical models using Richards' equation and the Advection-Dispersion equation (ADE). Their analysis was based on intensive soil profile sampling that was conducted across the LPC, which enabled the use of a detailed modeling approach. However, the physical soil properties were mostly obtained from the shallow depths of the LPC. This limited the examination of the effect of vertical loess vadose zone variability on model simulation results. Furthermore, Turkeltaub et al. (2020) compared the detailed approach with estimates derived from global scale models that are based on simple approaches (piston flow). The discrepancies in nitrate travel times and recharge fluxes were partly explained by the simplistic representation of the flow processes. Recently, Jia et al., (2018) presented deep vadose zone nitrate concentration profiles at five study sites across the LPC. Valuable additional information regarding the loess physical properties were collected during the study of Jia et al. (2018). Given the paucity of such deep vadose zone datasets, these data give us the rare opportunity to explore the possible effect of loess vertical variability and the level of model complexity on unsaturated water flow and nitrate transport in the LPC. Thus, the objective of this study is to assess the model complexity needed to predict site-specific nitrate accumulation and migration within deep loess vadose zone profiles.

2 Method

2.1 Study area

Loess is an aeolian deposit that evolved mainly during the Quaternary and covers 10% of the Earth's surface (Smalley et al., 2011). The loess sediments are dominated by silt grain size, often resulting in a limited spatial variability of the loess properties (Smalley & Marković, 2014). The rich amount of silt within the loess sediments makes it effective for agriculture production (Catt, 2001). Additionally, in many cases, unconfined groundwater systems are located under or within of the loess deposits (El Etreiby & Laudelout, 1988). Numerous studies have investigated the possible impact of intensive agricultural cultivation on water quality of the loess groundwater systems (Baran, et al., 2007; El Etreiby & Laudelout, 1988; Huang et al., 2013; Isla et al., 2018; Keller et al., 2008; Wagner & Roberts,1998).

The LPC region covers a total area of 0.64×10^6 km^2, where a continuous loess has an area of 0.43×10^6 km^2, accounting for about 72% of the loess-covered area in China (Jia et al., 2015, Figure 1). This region is subject to a semiarid to subhumid climate; most rain (55–78%) falls in the form of high intensity rainstorms between June and September. According to daily climate data that were obtained in the vicinity of four study sites investigated here (Figure 1; State

Bureau of Meteorology, 2018; http://cdc.cma.gov.cn), the total annual precipitation ranges between 420 mm in Shenmu (north, Figure 1) and 627 mm in the Yangling (south, Figure 1). The annual estimated evapotranspiration is between 928 mm at Yangling and 1028 mm at Shenmu and the mean annual temperature ranges from 9°C in Shenmu to 13.3°C in Yangling (Figure 1). An unconfined aquifer is embedded within the loess sediments and the water table is located on average at 52 m depth but can vary between 0 and 233 m according to the model of Fan and Miguez-Macho (2013). This groundwater resource has been overexploited, and the regional water table is rapidly declining, between 0.5 and 1 m per year (Huang & Pang, 2011; Li et al., 2014).

The loess is comprised of lower Pleistocene (Wucheng Loess), middle Pleistocene (Lishi Loess), and upper Pleistocene (Malan Loess) (Kukla, 1987; Derbyshire, 2001; Huang & Pang, 2011). The Malan Loess typically has a thickness of up to about 10 m and is distributed as the topsoil in the area. This loess type is characterized by a bulk density (BD) of 1.34 g/cm^{-3} and a saturated hydraulic conductivity (Ks) of 35 cm/day (Derbyshire, 2001). Underlying the Malan Loess is the Lishi loess, with a typical thickness of 120–150 m, a BD of 1.58 g/cm^{-3} and a Ks of 4.6 cm/day (Derbyshire, 2001). The LPC regional unconfined aquifer is embedded within the Lishi Loess. The Wucheng Loess, with a thickness of 40–60 m, is hard and compacted, resulting in low permeability and is consequently usually considered as an aquitard (the BD is about 1.68 g/cm^{-3} and the Ks is 1.27 cm/day; (Derbyshire, 2001)).

The deep vadose zone data that are utilized in this study were extracted from four sites along a south-north direction across the Loess Plateau of China (LPC): Yangling, Changwu, An'sai and Shenmu (Jia et al., 2018; Figure 1). According to Jia et al. (2018), at the Yangling site a double cropping system has been implemented, where wheat is cultivated during winter (October to May) and corn during summer (June to September). Because of the intense agricultural cultivation and the lack of substantial rain events during winter, the wheat crop has to be irrigated (Huang et al., 2004). Wheat and corn are also cultivated at the Changwu site, however, only a single crop is cultivated each year. At the An'sai site a single crop cultivation system is implemented, with rotation between millet and soybeans. The Shenmu site is currently covered with grass, although it was cultivated until the end of the 1990s (Jia et al., 2018). Note that Changwu, An'sai and Shenmu sites are rainfed, i.e. no irrigation is applied.

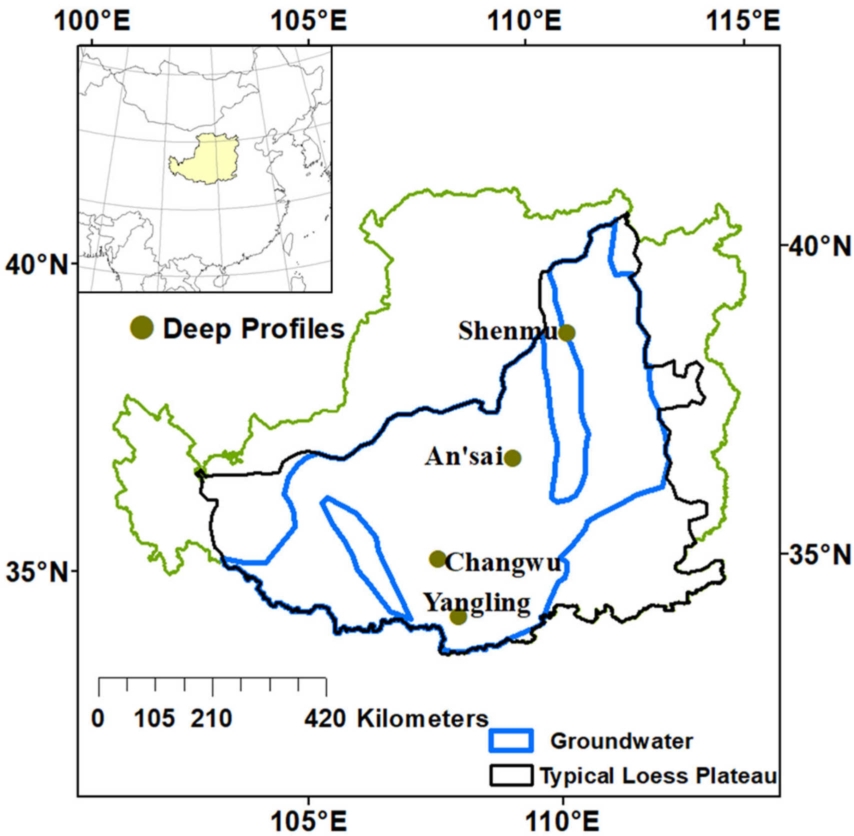

Figure 1. *The Loess Plateau of China is marked by the green line and the subregion of continuous loess is indicted by the black line. The blue line designates the approximate boundaries of the unconfined groundwater system modified from Huang et al., (2013). The green circles represent the four study sites where deep boreholes were drilled (Jia el al., 2018).*

2.2 Loess properties and nitrate concentrations in deep vadose zone

A full description of the soil sampling and soil physical analysis relating to data used here can be found in Jia et al. (2018), and, therefore, only a brief explanation of the database is given here. The deep vadose zone profiles were drilled (15 cm diameter borehole) from the land surface to bedrock between May and June 2016, using the under-reamer method (Overburden Drilling

Exploration; Izbicki et al., 2000). As this study focuses only on the unsaturated zone, data collected below the water table is not considered. The water tables are located at 81, 96, 141 and 54 m depth in Yangling, Changwu, An'sai and Shenmu, respectively. For the Changwu, An'sai and Shenmu sites, soil cores were sampled at 1m intervals, while at the Yangling site soil cores were taken every 0.5 m to a depth of 10 m, and at 1 m intervals for depths beyond 10 m. The samples were analyzed for gravimetric water content, particle size distribution, bulk density, pH, NO_3-N and NH_4-N and ^{15}N and ^{18}O in nitrate. For further details, the reader is referred to Jia et al. (2018). Note that the volumetric water contents were computed from the gravimetric water content and bulk density. For clarity, the data are elaborated below briefly.

Figure 2 shows the vertical variability of the particle size distribution (PSD) at the four study sites, organized from south to north of the LPC (Figure 1). The PSD data clearly confirm the predominance of the silt fraction for all sites. Nevertheless, there is a distinguished increase in sand fraction and decrease in silt and clay fractions with depth from Yangling (south) to Shenmu (north), which is accordance with previous regional studies that investigated distribution of loess particle size extensively (e.g. Derbyshire, 2001).

The bulk density measurements show a more complex behavior compared to the textural information (Figure 3). An increase in bulk density from soil surface to about 10 m depth can be seen at all sites. Note that the depth where the bulk density stabilizes is different for each site. Moreover, some transitions in bulk density can be observed at depth (e.g., 40 m at Yangling). This phenomenon was not reported previously and its effect on the water flow in the vadose zone is unknown. As is illustrated by Derbyshire (2001), the bulk densities are expected to show an increase with depth, where the Malan loess type changes to the Lishi loess type.

Relatively high nitrate concentrations occur in the vadose zone of the Yangling and Changwu sites (Figure 4a,b). Nitrate accumulation is observed at about 50 m and 30 m depth in Yangling and Changwu, respectively, which is the deepest recorded vadose zone nitrate transport in loess, under rainfed and irrigated land uses. Analysis of nitrate isotopes by Jia et al. (2018) showed that a significant proportion of the nitrate is of anthropogenic origin. Furthermore, previous studies on nitrate in vadose zone of loess in China (Huang 2013) and elsewhere, e.g. France (Baran et al, 2007), revealed long travel times of nitrate in the vadose zone. Therefore, the detection of nitrate at very deep depths under the Yangling and Changwu sites is rather unique. At the other sites, nitrate accumulation appears to be low and relatively far from the water table (Figure 4c,d,e).

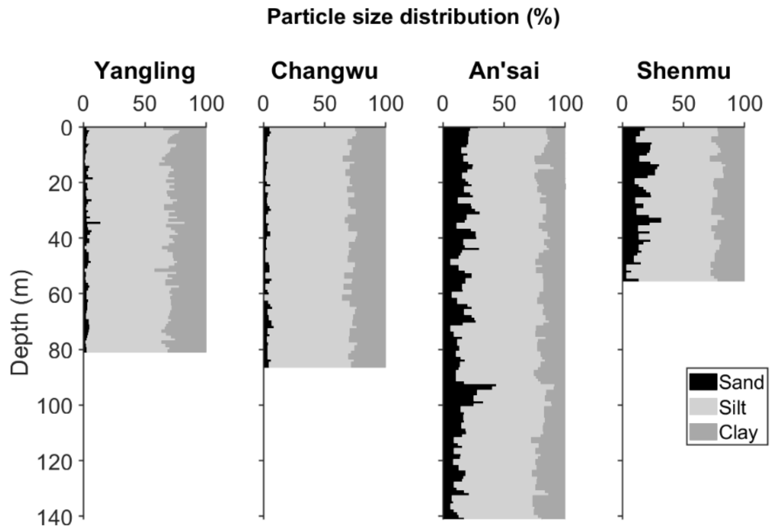

Figure 2. *The depth profiles of particle size distribution for the four sites across the Loess Plateau. Note that the water tables are located at the bottom of each profile.*

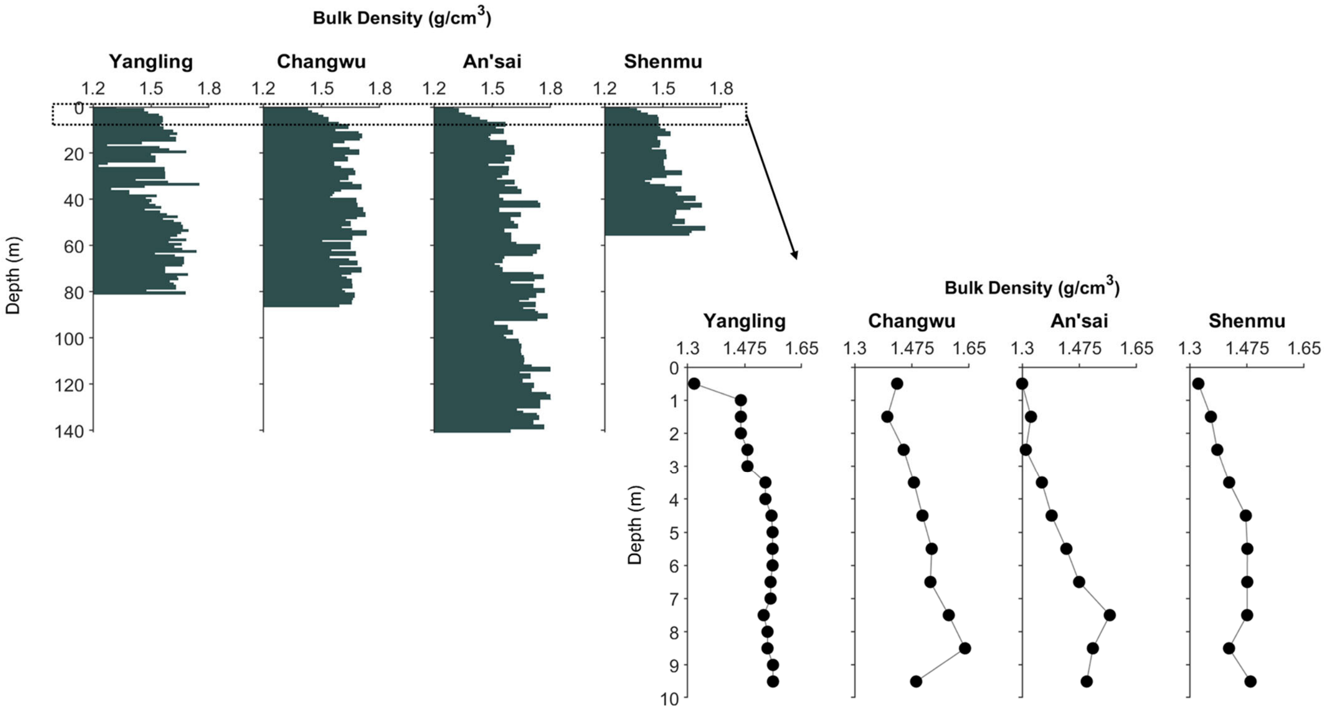

Figure 3. *The vertical bulk density distribution for the four sites across the Loess Plateau.*

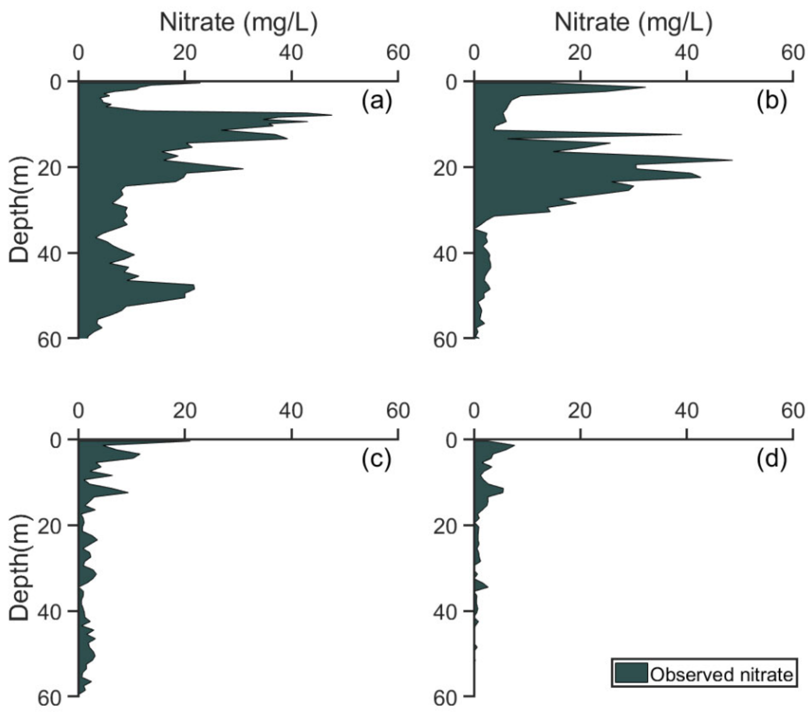

Figure 4. *The vertical nitrate distribution in the vadose zone of: (a) Yangling, (b) Changwu, (c) An'sai and (d) Shenmu.*

2.3 Soil hydraulic functions

Soil retention curves and unsaturated hydraulic curves are commonly described according to the van Genuchten-Mualem (VGM) model (Mualem, 1976; van Genuchten, 1980):

$$S_e = \frac{\theta-\theta_r}{\theta_s-\theta_r} = [1 + (\alpha|\psi|)^n]^{-m}, \quad (1)$$

where S_e is the degree of saturation ($0 < S_e < 1$), θ_s [L^3 L^{-3}] and θ_r [L^3 L^{-3}] are the saturated and residual volumetric soil water contents, respectively, α [L^{-1}], n [-], and $m = (1 - 1/n)$ are shape parameters.

Hydraulic conductivity is often described by:

$$K(S_e) = Ks \times S_e{}^l\left[1 - [1 - (S_e)^{1/m}]^m\right]^2, \quad (2)$$

where Ks [L T^{-1}] is the saturated hydraulic conductivity and *l* is the pore connectivity parameter prescribed as 0.5.

Three undisturbed soil cores were collected from the upper 10 cm of the soil at each of the four deep vadose zone study sites (Figure 1, green circles). Subsequently, three soil retention curves were measured for each site using the Hyprop system (UMS GmbH, Munich, Germany). The VGM parameters were obtained using the *lsqcurvefit* function in MATLAB optimization toolbox. Ks values were extracted from the nearest sampling point of earlier regional studies (Wang et al., 2013b; Jia et al., 2015). In the regional studies, undisturbed soil cores were collected from depths between 0 and 25 cm and Ks was determined using the constant head method. For the deeper parts of the investigated deep vadose zones, only particle size distribution and bulk density information were available. To estimate the VGM parameters, the Rosetta3 pedo-transfer function (PTF) was applied (Zhang & Schaap, 2017). The Rosetta3 PTF relates simple-to-measure soil properties and the VGM parameters. Five different PTFs are included in Rosetta3, which enable the estimation of VGM parameters from different levels of information according to available data. In the current study the second model of Rosetta3, which uses the loess texture and bulk density data (Figures 2 and 3), was implemented.

Table 1. *Fitted van Genuchten -Mualem soil parameters against observed retention curves using the Hyprop system. The soil cores were obtained from 10 cm depth at each study site (the observed and fitted retention curves are included in the Supporting Information). The Ks values were extracted from the nearest sampling point of previous regional studies (Wang et al., 2013b; Jia et al., 2015).*

Site	θ_r (cm^3/ cm^3)	θ_s (cm^3/ cm^3)	α (1/cm)	n	Ks (cm/day)
Yangling	0.186	0.526	0.054	1.63	16
Changwu	0	0.52	0.0128	1.41	51
An'sai	0.086	0.5	0.0084	2.24	81
Shenmu	0.023	0.35	0.0017	1.89	61

2.4 Ks vertical decay

A relatively simple approach to determine soil vertical variability is by considering the gradual decrease of the saturated hydraulic conductivity, Ks, with depth (Beven and Kirkby, 1979; Jiang et al., 2009; Ameli et al., 2016). Wang et al. (2017) indicated that Ks in the loess plateau shows a decreasing trend with depth due to compression effect. Moreover, they suggested that this trend can be expressed with an exponential decay function:

$$Ks(z) = (Ks_0 - Ks_1) \times exp^{-\frac{z}{z_f}} + Ks_1, \qquad (3)$$

where Ks_0 [L/T] is the saturated hydraulic conductivity at the top of the soil profile, Ks_1 [L/T] is the saturated hydraulic conductivity at infinite depth, z_f [L] is a fitting parameter and z [L] is the soil depth. Equation 3 is fit to the vertical distribution of Ks values predicted by the Rosetta3 PTF model.

2.5 *Scaling factors of the hydraulic functions*

To account for the vertical variability of the soil properties, several earlier deep vadose zone studies have suggested the application of the Miller-Miller scaling approach (Miller & Miller, 1956; Nimmo et al., 2002; Botros et al., 2012). The basic assumption of the Miller-Miller approach is that when two porous media share similar geometry, they can be scaled through a physical characteristic length (Miller & Miller, 1956; Sadeghi et al., 2016). The heterogeneity of the soil is then expressed by a single set of scaling factors (simultaneous scaling) that relates the local properties to a reference set of hydraulic functions as follows (Clausnitzer et al., 1992):

$$h(S_e)_i = \frac{\hat{h}(S_e)}{\delta_i} \tag{4}$$

$$K(S_e)_i = \delta_i^2 \times \hat{K}(S_e) \tag{5}$$

where δ_i is the scaling factor for the hydraulic functions of a soil at depth *i*, $\hat{K}$ and $\hat{h}$ are the reference water retention and unsaturated hydraulic curves, respectively, $K(S_e)$ and $h(S_e)$ are the hydraulic functions at depth *i*. The degree of saturation (S_e) is used to avoid the need to assume identical porosities. To calculate the individual scaling factor (δ_i) throughout the loess vadose zone, an objective function ($\Phi(p)$) was establish to minimize the differences between the reference hydraulic curves and the hydraulic curves estimated from Rosetta3 for each depth *i*. Note that the fitted hydraulic parameters in Table 1 were assumed to represent the reference hydraulic curves. The objective function is as follows (Clausnitzer et al., 1992; Nasta & Romano, 2016):

$$\min \Phi(p) = min \sum_{i=1}^{I} \Phi(p)_i \tag{6}$$

$$\Phi(p)_i = WH_i \sum_{\eta=1}^{N} \left[\hat{h}(S_e)_\eta - h(S_e)_{\eta,i}\right]^2 + WK_i \sum_{\eta=1}^{N} \left[ln(\hat{K}(S_e)_\eta) - \ln\left(K(S_e)\right)_{\eta,i} - 2\ln(\delta_i)\right]^2, \tag{7}$$

where *p* is the parameter vectors that includes all scaling factors, N denotes the number of values of the degree of saturation, S_e, ranging from 0 to 1. Note that only the soil hydraulic functions parameters were available. Therefore, the $h_{i,\eta}$ and $K_{i,\eta}$ were estimated by implementing a range of S_e values in the VGM models. Equation 7 was solved using the *fminsearch* function in MATLAB toolbox.

3 Setup of Models

Two modeling approaches are implemented in this study to describe the migration of water and nitrate in the deep loess vadose zone. The first is a piston flow and nitrate mass balance model based on the work of Laio et al. (2001), Porporato et al. (2003) and Guswa et al. (2002). The second is the one-dimensional Richards' equation and one-dimensional ADE with nitrate reactions.

3.1 Piston flow model and nitrate mass balance model (PFMB)

Water balance in absence of surface runoff can be described by (Laio et al., 2001; Guswa et al., 2002; Romano et al., 2011):

$$n_p Z_r \frac{dS}{dt} = P - ET - R \qquad (8)$$

where dS/dt is the water storage change over time, S is the average saturation over the root zone, n_p is the porosity, Zr is the depth of the root zone, P [L/T] is the precipitation, R [L/T] is the percolation (potential recharge) at the profile bottom and ET [L/T] is the evapotranspiration (ET). The ET is composed of the soil evaporation (E) and transpiration (T, root water uptake). Here, the water balance was calculated at a daily resolution.

The transpiration rate is controlled by two mechanisms: the atmospheric demand and the supply of water in the soil. Assuming that there is no effect of salts, the uptake function can be described by:

$$T(S) = \left\{ \begin{matrix} 0 & S \le S_w \\ \frac{S - S_w}{S^* - S_w} * T_p & S_w < S < S^* \\ T_p & S \ge S^* \end{matrix} \right\} \qquad (9)$$

where T_p represents the maximum transpiration rate as dictated by the atmospheric demand, S^* is a threshold value and S_w is the saturation at which the uptake is zero and the plant wilts.

Evaporation from the root zone is described similar to the root water uptake approach:

$$E(S) = \begin{Bmatrix} 0 & S \leq S_h \\ \frac{S-S_h}{S^*-S_h} * E_p & S_h < S < S^* \\ E_p & S \geq S^* \end{Bmatrix} \quad (10)$$

where S_h is the hygroscopic saturation, at which evaporation ceases. Note that the average saturation at which E reaches its maximum, S^*, is the same as that for transpiration (equation 9).

As described by Laio et al. (2001), drainage of the root zone (potential recharge) is set equal to the unsaturated hydraulic conductivity, described with an exponential form:

$$R(S) = Ks \times \frac{e^{\beta(S-S_{fc})}-1}{e^{\beta(1-S_{fc})}-1} \quad (11)$$

where Ks is the saturated hydraulic conductivity, β is a parameter of the soil and S_{fc} is the field capacity.

The nitrate leaching rate is calculated simultaneously to the water balance approach according to the following mass balance approach:

$$NO_{3_{Leaching}} = NO_{3_{Input}} - NO_{3_{Soil}} - NO_{3_{Uptake}} \quad (12)$$

The nitrate mass balance approach is based on the assumption that three main processes control the nitrate dynamics in the root zone; passive nitrate uptake ($NO_{3\ Uptake}$), and nitrate leaching ($NO_{3\ Leaching}$). Note that the $NO_{3\ Soil}$ represent the residual nitrate in the root zone and $NO_{3\ Input}$ is the fertilizer amount.

The passive nitrate uptake is assumed to be proportional to the transpiration rate, T(s) in equation 9, and to the nitrate concentration in the soil solution:

$$NO_{3_{Uptake}} = \frac{T(S)}{n_p S Z_r} C_{NO_3} \quad (13)$$

where Zr [L] is the depth of the root zone and C_{NO_3} [M/L^2] is the nitrate concentration within the root zone. Nitrate leaching is assumed to be proportional to the recharge term $R(S)$ modeled in equation 11,

$$NO_{3_{Leaching}} = C_{NO_3} \times exp^{((-k_l \times R(S))/n_p)} \quad (14)$$

where k_l is the leaching coefficient and equals to 0.02 in the current study.

To calculate vertical nitrate displacement in the vadose zone using the piston flow approach, pore water velocities are estimated using the recharge fluxes (R). Water velocities are linearly related to the calculated water fluxes by a coefficient that represents the specific volume through which the water and solutes are transported. Assuming only vertical advective transport of nitrate in the loess unsaturated zone, the displacement ΔZ of the nitrate is given by:

$$\Delta Z = R(t) \times \Delta t \times n_p \quad (15)$$

where $R(t)$ is the (time-dependent) recharge, and Δt is the time step. The n_p parameter in this study was set to the average measured water contents in the vadose zone of each of the study sites (Figure 1).

The piston flow and nitrate mass balance model were calibrated against the total nitrate storage calculated from the nitrate profiles in Figure 4 and the observed water contents (see *Supporting Information*). Only the β parameter in equation 11 was modified during the calibration process.

3.2 Richards' equation and one-dimensional ADE

The numerical modeling approach is based on Richards' equation and the ADE with nitrate reactions. This approach was implemented with three different degrees of complexity in describing vertical loess heterogeneity. To determine the unsaturated flow in the loess, the 1D vertical Richards' equation was implemented with a root water uptake sink as follows:

$$\frac{\partial \theta}{\partial t} = \frac{\partial}{\partial z}\left[K(\psi)\left(\frac{\partial \psi}{\partial z} + 1\right)\right] - RWU, \qquad (16)$$

where ψ is the matric potential head [L], θ is the volumetric water content [$L^3\ L^{-3}$], t is time [T], z is the vertical coordinate [L], $K(\psi)$ [$L\ T^{-1}$] the unsaturated hydraulic conductivity function, is a function of the matric potential head and RWU is a root water-uptake sink term [$L^3\ L^{-3}\ T^{-1}$]. The Richards equation was solved numerically by using the Hydrus 1D code (Šimůnek et al., 2008). Simulation of the root water uptake rate (the sink term) was conducted according to the model suggested by Feddes et al. (1978). The parameters used for the different plant types were obtained from the Hydrus 1D database.

The following set of equations was used to model the 1D vertical transport of NO_3:

$$\frac{\partial \theta C_{NO_3}}{\partial t} = \frac{\partial}{\partial z}\left[\theta D \frac{\partial \theta C_{NO_3}}{\partial z}\right] - \frac{\partial q C_{NO_3}}{\partial z} - f_{NO_3} S C_{NO_3}, \qquad (17)$$

where C_{NO3} [M L^{-3}] is the concentration of nitrate in the pore-water solution, D [L^2 T^{-1}] is the hydrodynamic dispersion coefficient, q [L T^{-1}] is the water flux, $f_{NO_3}SC_{NO_3}$ [M T^{-1} L^{-3}] is the root NO_3 uptake sink, where f_{NO_3} is a function relating solute uptake to the water uptake S and solute concentrations. The nitrate uptake rate values were prescribed according to previous studies (Hanson et al., 2006; Ramos et al., 2011; Kurtzman et al., 2013; Turkeltaub et al., 2018).

Vanderborght & Vereecken (2007) established a linear relationship between longitudinal dispersivity (λ) and travel distance in soils under unsaturated conditions (up to 1.2 m). The slope of their relationship is 0.046, i.e. the dispersivity can be considered to be approximately 5% of the soil profile thickness. In contrast, Hillel (1998) proposed that λ should be considered to be 10% of the soil's column length. In this study, the dispersivity values were prescribed according to the latter suggestion for simulations with no model calibration (see model calibration section).

The spatial distribution of root density with depth was assumed to follow the exponential model presented by Vrugt et al. (2001):

$$\beta(z) = \left[1 - \left(\frac{Z}{Z_m}\right)\right] - e^{\frac{P_Z}{Z_m}|Z^* - Z|}; \quad Z \geq 0, \qquad (18)$$

where $\beta(z)$ denotes the dimensionless spatial root distribution with depth, z_m is the maximum rooting depth [L], and p_z [-] and z^* [L] are empirical parameters. Maximum root depth (z_m) values were prescribed according to earlier studies in the LPC and a global study (Canadell et al., 1996; Huang et al., 2004; Wang et al., 2013a; Fan et al., 2016). The fitting parameters (p_z and z^*) were prescribed according to Turkeltaub et al. (2018).

3.3 *Numerical model concept, evaluation, and calibration*

To characterize subsurface heterogeneity three conceptual models were examined and compared. For the simplest model (HOM model), the topsoil fitted VGM parameters are prescribed, assuming uniform (homogenous) soil profiles (Table 1). In the second model (EXP), the Ks decay function (equation 3) is prescribed to account for the exponential decay of the hydraulic conductivity function with depth. For the third model (HET), the Miller- Miller factors (equations 4 and 5) are used to account for the vertical heterogeneity of the retention and the hydraulic conductivity functions with depth.

The three conceptual models were calibrated against water content profiles (*Supporting Information*) and nitrate profiles (Figure 4) obtained from the loess vadose zones. An inverse problem was formulated to find an optimum combination of parameters that minimizes the following objective function:

$$\Phi(b) = \sum_{i=1}^{N} w_i[\theta(z_i) - \theta(z_i, b)]^2 + v_i[C\_NO_3(z_i) - C\_NO_3(z_i, b)]^2, \qquad (19)$$

where N is the number of the water content and nitrate concentration observations, $\theta(z_i)$ or $C\_NO_3(z_i)$ are the observations at specific depth, and $\theta(z_i,b)$ or $C\_NO_3(z_i,b)$ are the corresponding model predictions for the vector of optimized parameters (VGM parameters). Note that the simulated water content and nitrate profiles at the end of each model run were implemented for the inverse calculations. The weighting factors w_i and v_i account for data type and are given by (Clausnitzer & Hopmans, 1995):

$$w_i = \frac{1}{N\sigma_\theta^2};\ v_i = \frac{1}{N\sigma_{\mathrm{C\_NO3}}^2} \qquad (20)$$

where σ^2 are the measurement variances. The inverse problem was solved using the *fminsearch* function in MATLAB toolbox. To reduce the parameter space, sensitivity tests were conducted before model calibration. The sensitivity tests were implemented individually for each of the parameters in Table 1 and for the λ parameter. Initially, the model simulation involved only the original parameter values (Table 1). Subsequently, each parameter was changed in a ±1% step until ±10%, thus in total there were 20 model runs. The model simulations calculated with the perturbed parameters were compared with the model output of the original (i.e. not changed) parameter. A sensitive parameter is defined here as one in which a change of the parameter produces a root mean squared error (RMSE) that is larger than the standard deviation of the original simulation, with *a priori* parameter estimates. Finally, the RMSE, mean error (ME) and r (correlation coefficient) were calculated to compare performances of the three different model approaches.

3.4 Climate and nitrogen inputs

The daily climate data extend from 1 January 1961 until 31 December 2014 (19,723 days), except for the An'sai site, where climate data were available until 31 December 2012 (18,993 days). These datasets include daily rain, daily mean, maximum and minimum air temperature, relative humidity, wind speed (m/s) and sunshine duration. The models were calculated at daily time steps. Note that for the numerical models there is a 'spin-up' period (see below).

Daily reference evapotranspiration (ET_0) was calculated according to the Penman-Monteith equation (Allen et al., 1998). To estimate the crop evapotranspiration (ET_c), the daily ET_0 values were multiplied with crop coefficients (Kc, Allen et al., 1998). Kc values for wheat and corn were retrieved from Kang et al. (2003), and the Kc values for millet, soybean and bare soil were based on Allen et al. (1998). Due to the double crop system at the Yangling site, irrigation was implemented during the wheat cultivation (Huang et al., 2004). Note that the other three sites are rainfed and no irrigation was implemented. Beer's law was implemented for partitioning of ET_c to evaporation and transpiration (Ritchie, 1972). The description of this approach is in the *Supporting Information*. Furthermore, Beer's law requires information regarding the change of leaf area index (LAI) with time. Thus, the change of LAI in the growing season for winter wheat, corn, millet, soybean and grassland was estimated with the model of Leenhardt et al. (1998) (see *Supporting Information*).

The N input in the models for the different sites was defined according to previous studies and personal communication (Fan et al., 2005; Jia et al., 2018). At Yangling, the total N inputs are assumed to be 300 kg/ha/year with a wheat-corn double cropping system. The N inputs in Changwu are estimated as 260 kg/ha/year for corn and 324 kg/ha/year for wheat. The Changwu site was abandoned in 1991 and is simulated as bare soil from this year. At An'sai and Shenmu, the assumed N input was 100 kg/ha/year, but N applications ceased in 1995 at the Shenmu site. Note that the cultivation history is not well documented for any of the sites, therefore the year of nitrate application was decided according to earlier investigations. The nitrogen was prescribed as nitrate concentration in the numerical model and in kg/ha in the mass-balance approach in one yearly application at the beginning of the growing season.

Atmospheric boundary conditions with surface runoff were prescribed at the upper boundary (land surface) of the numerical models. Previous studies have illustrated that the effect of water content initial conditions can be minimized by imposing periods of wet and dry conditions (Albertson & Kiely, 2001). To determine the spin-up time for the models, the expected unsaturated water travel times were considered. Turkeltaub et al. (2018) showed that the estimated water velocity across the LPC is 0.59 ± 0.48 m/year. Thus, it requires between 60 and 1300 years for water to pass through the vadose zone in the current study. To ensure that the simulated loess columns encountered at least one wetting and drying period, the atmospheric boundary conditions were replicated between 5 and 10 times, depending on the soil parameters and the amount of the water input (precipitation and irrigation). The nitrate initial conditions were prescribed zero concentration, assuming no accumulation of nitrate before the start of the actual simulation.

It is difficult to implement mixed cropping systems in the Hydrus 1D code. Therefore, the models for the Yangling and Changwu sites were run with the root uptake and density parameters for a corn crop, but the upper boundary conditions (i.e. LAI, Kc, nitrogen (as nitrate concentration) application and irrigation) were set according to wheat and corn. A similar approach was implemented for the An'sai site, but with millet and soybean crops, with the root uptake and density parameters set for millet crop type.

4 Results

4.1 Piston flow and nitrate mass balance (PFMB) estimations

Table 2 shows the calibrated β parameters for the four sites, the total nitrate storage in the vadose zone and the RMSE values comparing observed nitrate storage in the loess vadose zones and the simulated storage. Additionally, the estimated recharge fluxes and nitrate leaching during cover and fallow times are presented (Table 2). According to the low RMSE values, it appears that the PFMB model predicts well the nitrate storage in the loess vadose zones. The β parameters illustrate a relatively wide range of values among the sites (Table 2). Laio et al. (2001) suggested that the β parameter for clay, loam and sand soil types should be about 26, 14 and 12, respectively. Other studies have reported a wider distribution of β values, between 5 and 27, with no obvious relation with the soil type (Guswa et al., 2002; Baudena et al., 2012). Therefore, the β parameter was considered to be a fitting parameter in the current study.

In Yangling, most recharge and nitrate leaching occurred during the cultivation periods (Table 2). These intensive fluxes during the crop period are probably due to irrigation that exceeds plant requirements. In Changwu, there is an alternation between wheat crop (winter cultivation) and corn (summer cultivation), where only one crop is cultivated each year. Therefore, in years where the wheat crop is cultivated, there is minor loss of water to transpiration during the intensive summer rainstorms (Table 2). The crops in An'sai are mainly cultivated during summer and the Shenmu site is covered with grass permanently. At these two sites, the suggested groundwater recharge is between 15 and 10% of the rain, similar to previous studies conducted under comparable conditions (Gates et al., 2011). The nitrate leaching fluxes illustrate that Yangling and Changwu are substantially over-fertilized.

By employing equation 15 and observed water contents, the vertical distribution of nitrate was estimated. Measured nitrate profiles are compared with simulated nitrate profiles in Figure 5. The comparison between the measured and the simulated nitrate profiles demonstrates that the PFMB model has only partly succeeded to reconstruct features of the measured nitrate concentrations. All simulated nitrate profiles show much larger concentrations and less vertical spreading (Figure 5). Nevertheless, the simulated large nitrate concentrations are located at similar locations where nitrate observations exhibit large concentrations (Figure 5). Thus, by implementing the PFMB model and assuming advective transport only, an approximate location of where nitrate is mostly stored in the vadose zone can be derived.

Table 2. *Calibrated β parameters, observed nitrate storage, RMSE evaluation of predictions, groundwater recharge fluxes and nitrate leaching fluxes as were simulated by the piston-flow mass balance model and the nitrate mass-balance approach.*

	β	RMSE (kg/ha)	Groundwater recharge (mm/year)	Nitrate leaching (kg/ha)

		Total observed nitrate storage (kg/ha)		fallow	cover	fallow	cover
Yangling	14.58	2968	0.7	18 ± 25	160 ± 113	2.4 ± 3.4	53 ± 37
Changwu	7.51	2756	0.13	190 ± 119	13 ± 33	47 ± 59	4 ± 13
An’sai	7.38	648	0.52	19 ± 22	72 ± 56	2 ± 3	10 ± 12
Shenmu	15.9	149	0.2	0	43 ± 68	0	3 ± 4

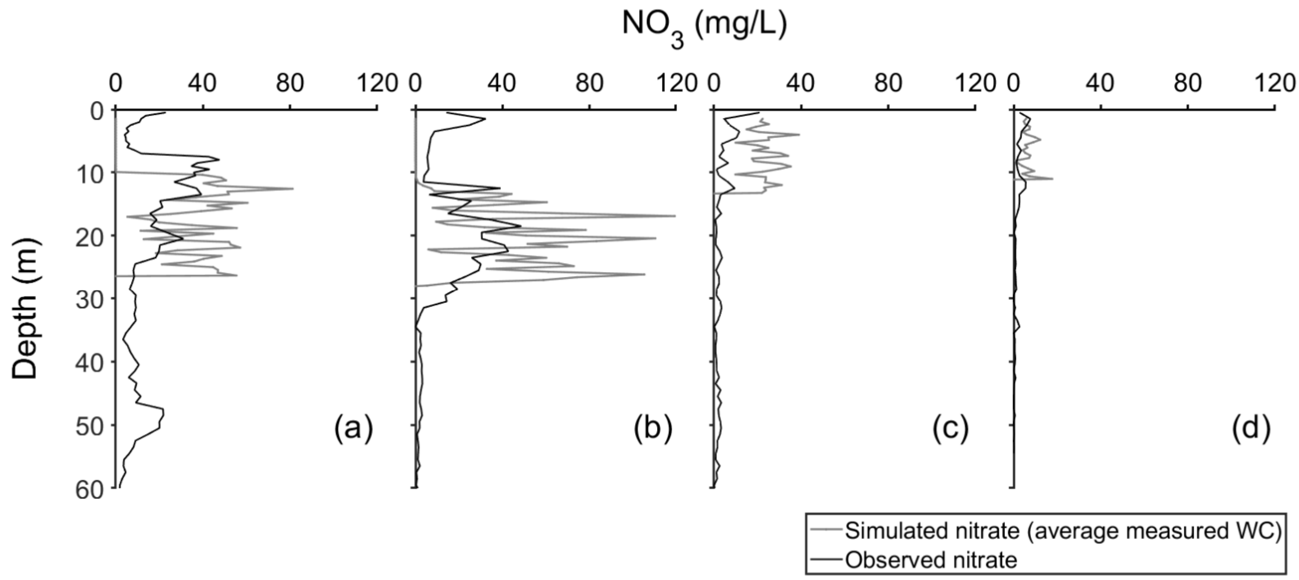

Figure 5. *A comparison between the simulated nitrate vertical distribution in the loess vadose zone estimated by the piston flow approach (PFMB) and the observed nitrate concentrations that were obtained at: (a) Yangling, (b) Changwu, (c),An’sai and (d) Shenmu. There is only an advective component in the PFMB model and pore-water velocity is calculated dividing the recharge by the average observed water content.*

4.2 Ks decay with depth

Derbyshire (1991) showed a linear relationship between bulk density of the different loess types and the saturated hydraulic conductivity (*Ks*). The vertical variability of the loess *Ks* was also studied in relation to slope stability (Derbyshire 1997; Wang et al., 2017). The decrease in *Ks* with depth is related to the (gradual) transformation from Malan loess type to Lishi loess type (Derbyshire, 2001). Wang et al. (2017) found a decay of *Ks* with depth up to about 13 m depth. Therefore, the vertical variability of the loess can be represented by a depth-decay function of *Ks*. In the current study, the values of *Ks* predicted by Rosetta3 show similar trends of gradual decrease with depth under the four sites (Figure 6). Although Rosetta3 is an artificial neural network model with a high level of complexity, the trend of the output *Ks* is obviously dictated by the bulk density measurements.

The reduction in *Ks* and the depth at which *Ks* values do not show further change are different for each site (Figure 6). Comparable values of Ks_1 (the saturated hydraulic conductivity at infinite depth) were estimated for all sites; 5, 4.1, 8.1 and 8.4 cm/day for Yangling, Changwu, An'sai and Shenmu, respectively. Furthermore, the estimated z_f values are 2.4 m, 4.8 m, 5.5 m and 6 m for Yangling, Changwu, An'sai and Shenmu, respectively. The *Ks* decay pattern, therefore, seems to be site specific (Figure 6). In addition, the cessation of the decay in Ks might indicate the reduction of the compaction effect; the reason why this is site specific is not clear.

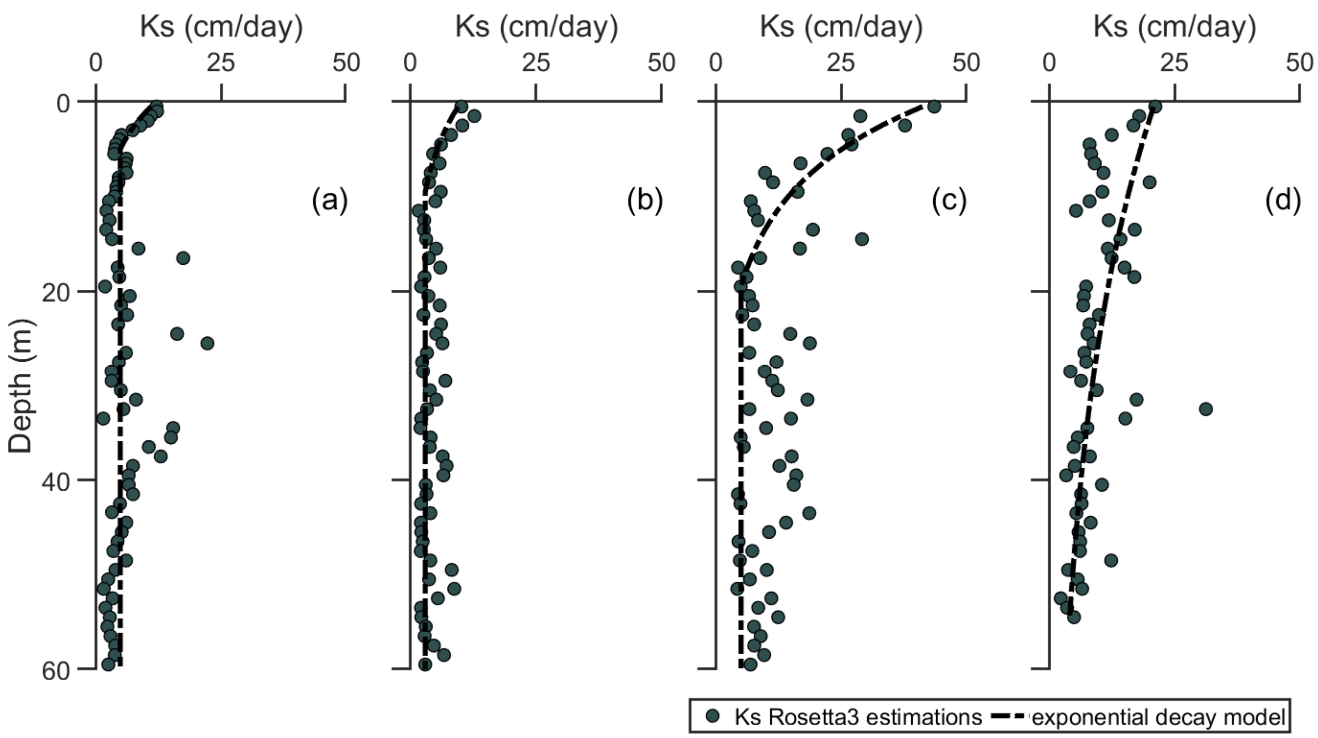

Figure 6. *Ks variation with depth under (a) Yangling (b) Changwu, (c) An'sai and (d) Shenmu. Note that the Ks values were estimated with Rosetta3, using particle size distribution and bulk density information. The black dash lines represent the exponential decay functions that were fitted to the estimated Ks values (see equation 3).*

4.3 Loess vertical scaling factors

The vertical variability of soil properties can also be described by Miller-Miller scaling factors. Firstly, the VGM parameters for soil samples from all depths were estimated using Rosetta3 based on the texture and bulk density data for each sampling point along the four vertical profiles (Figures 2 and 3). A single set of scaling factors for each site were calculated by applying equations 4 to 7. The unsaturated hydraulic functions in Table 1 were used as the reference curves.

The scaling factors mostly ranged between 0.2 and 0.8, which indicates that there is no strong contrast of the soil physical properties with depth (Figure 7). In general, the scaling factors display higher values close to the loess surface and a decrease with depth, which is similar to the observed trend of the bulk density measurements along the profiles. The scaling factors of the Yangling site show slightly higher values and variability compared to the other sites (Figure 7a). Note that the Yangling site is differ from the other sites by the climate conditions (higher temperature, ET and rain) and this site is also intensively cultivated (double cropping system). The agriculture cultivation might affect the variability of the near surface loess (e.g., accumulation of organic matter that changes the bulk density), while the effect of climate can be encountered throughout the loess vadose zone. However, the current analysis cannot indicate the dominant factor that generates the large variability in scaling factor at the Yangling site. Further study is required to elaborate and separate between the effect of agriculture land uses and the effect of climate on loess vertical variability.

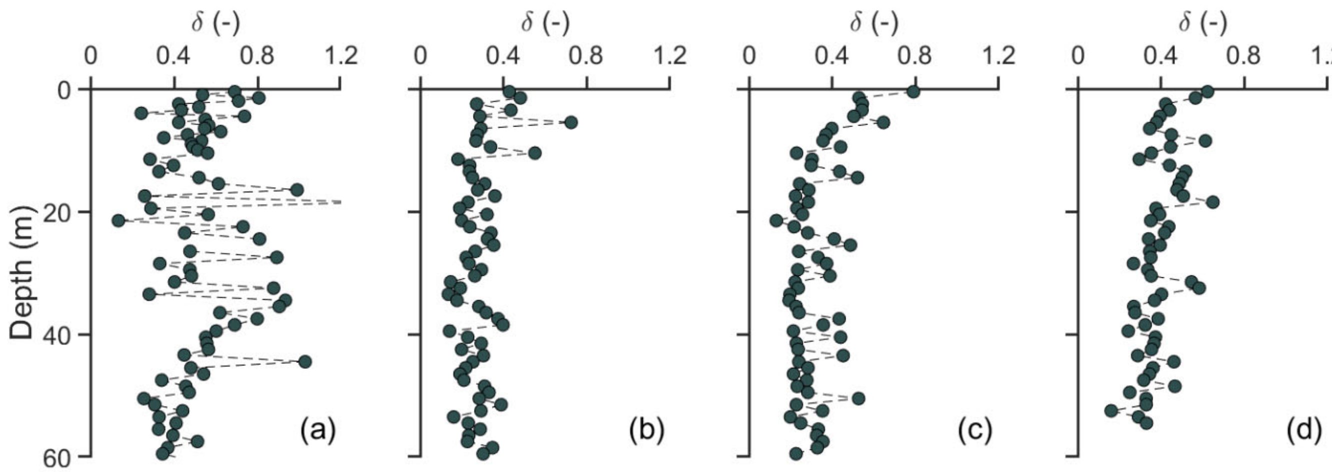

Figure 7. *Calculated scaling factors for: (a) Yangling, (b) Changwu, (c),An'sai and (d) Shenmu. The scaling factors were calculated using equations 4-7, topsoil fitted retention curves and estimated VGM parameters for each depth using Rosetta3.*

4.4 Calibration of the Numerical Models

In a next step, simulations using three different model approaches ((1) HOM, (2) EXP, and (3) HET) are examined and compared. All three models were further calibrated against the water content and nitrate observations (Figures 9 and 10). The calibrated parameters are documented in *Supporting Information* (Table S1). Sensitivity tests showed that the parameters n and θ_s in equations 1 and 2, are the most sensitive for all sites. However, to improve model performances, the Ks parameters were also included in the calibration process. In Changwu and Shenmu sites, the longitudinal dispersivity (λ) parameter was also included as a calibration parameter. Statistical evaluation of model performance is summarized in Tables 3 and 4. To explore the contribution of accounting for the loess vertical variability in the modeling, the statistics of model performances prior to calibration are also shown (Table 3 and 4).

The observed water content profiles from the four sites are plotted together with the simulated values from the three model configurations in Figure 8. In general, the simulated water content is within the same range as the observed volumetric water contents. Nevertheless, according to the evaluation results in Table 3, the EXP model that includes the Ks decay function produces a relatively better performance compared with the HOM and HET models for all sites. In fact, the HET model shows the poorest performance (Table 3). A comparison between evaluation results before and after calibration illustrates that calibration is necessary for most cases to improve model performance.

The results of the nitrate simulations are less conclusive (Figure 9, Table 4). Essentially, all models show vertical nitrate distributions that are similar to the observed nitrate profiles (Figure 9). Here, as before, the HET model displays the poorest performance. The HOM shows similar or slightly better performance relatively to the EXP model for all sites (Table 3, Figure 9). When comparing between the evaluation results of calibrated and uncalibrated models, for the Changwu, An’sai and Shenmu sites, the calibration procedure improves model simulations. However, for Yangling site no changes in the simulation results are apparent.

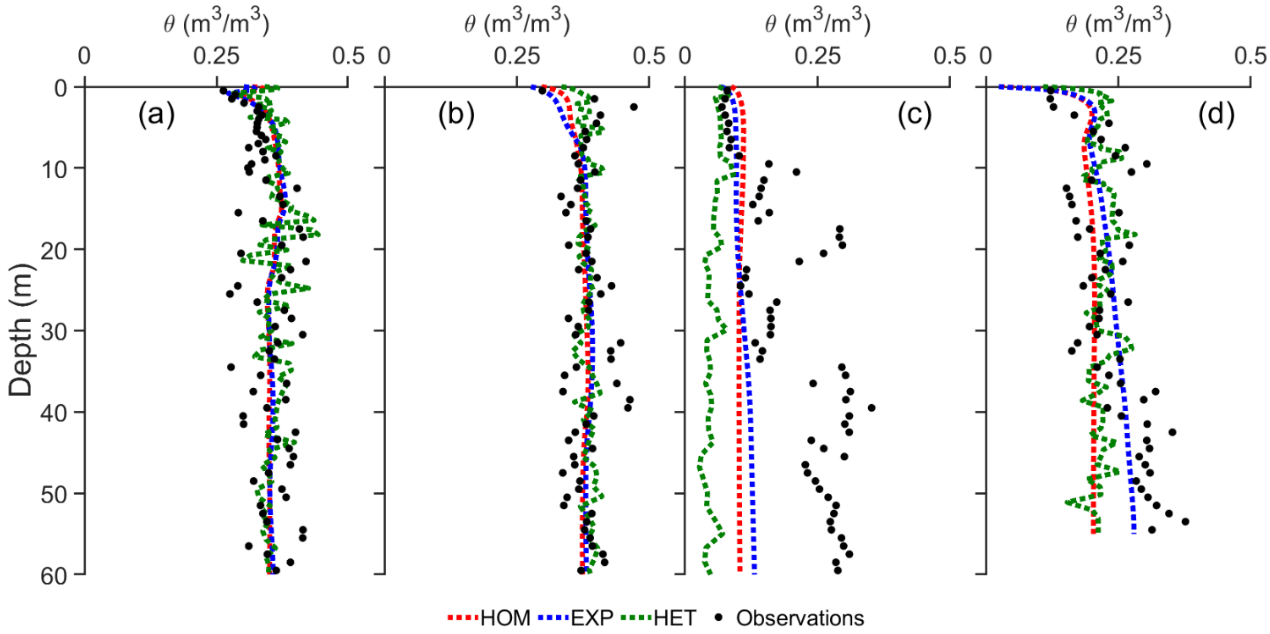

Figure 8. *Profiles of the measured water content, and the simulated water content as were calculated by the three approaches, HOM, EXP and HET after calibration for (a) Yangling (b) Changwu, (c) An'sai and (d) Shenmu.*

Table 3. *Evaluation results of the water content profiles as were simulated by the three conceptual models (Figure 8). In the rows, three different evaluation metrics are shown; from top to bottom, these are the mean error (ME), root mean squared error (RMSE), and correlation coefficient (r).*

		Calibrated			Not calibrated		
	Evaluation metrics	HOM	EXP	HET	HOM	EXP	HET
Yangling	ME	-0.004	-0.002	0.006	-0.012	-0.038	0.024
	RMSE	0.038	0.038	0.047	0.04	0.055	0.054
	r	0.3	0.34	0.071	0.24	0.29	0.06
Changwu	ME	0.013	0.0001	-0.002	0.097	0.07	0.19
	RMSE	0.036	0.036	0.037	0.10	0.08	0.19
	r	0.11	0.053	-0.14	0.098	0.08	-0.097

An'sai	ME	0.056	0.02	0.05	0.09	0.02	0.14
	RMSE	0.091	0.06	0.1	0.12	0.07	0.17
	r	0.72	0.82	0.02	0.69	0.82	-0.06
Shenmu	ME	0.041	0.001	0.022	0.15	0.13	0.17
	RMSE	0.072	0.047	0.075	0.16	0.14	0.18
	r	0.36	0.68	-0.29	0.31	0.76	-0.25

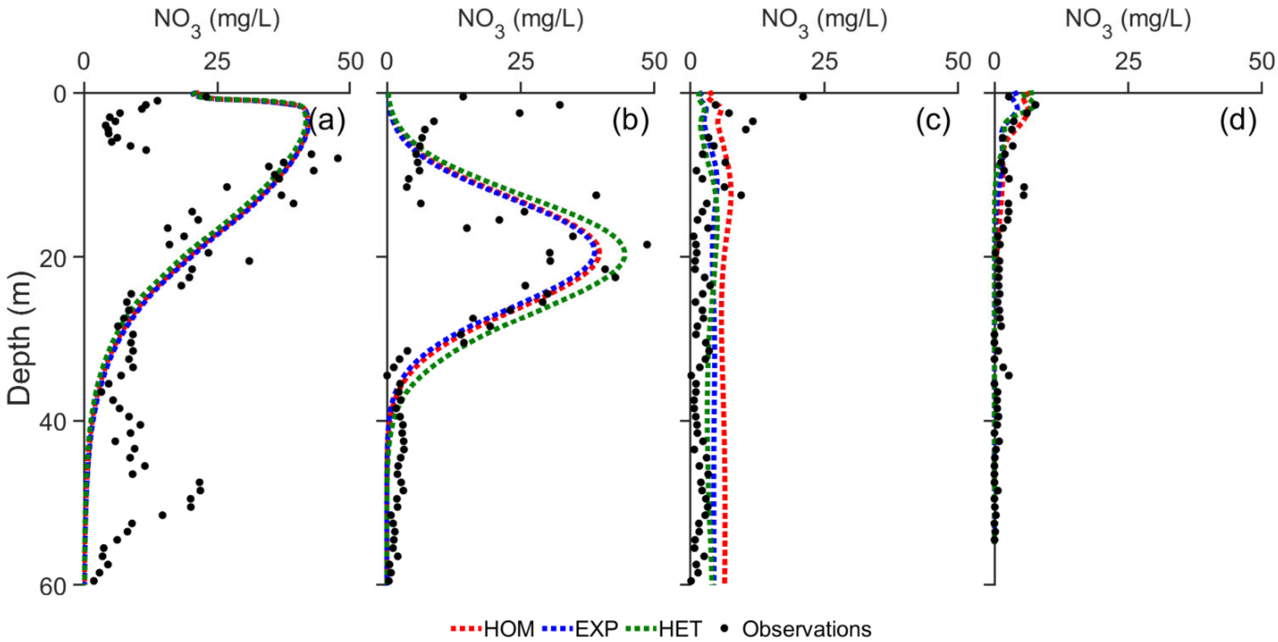

Figure 9. *Profiles of the measured nitrate concentrations, and the simulated nitrate concentrations as were calculated by the three approaches, HOM, EXP and HET after calibration for (a) Yangling (b) Changwu, (c) An'sai and (d) Shenmu.*

Table 4. *Evaluation results of the nitrate profiles as were simulated by the three conceptual models (Figure 9). In the rows, three different evaluation metrics are shown; from top to bottom, these are the mean error (ME), root mean squared error (RMSE), and correlation coefficient (r).*

	Calibrated	Not calibrated

	Evaluation metrics	HOM	EXP	HET	HOM	EXP	HET
Yangling	ME (mg/L)	-4.94	-5.37	-5.39	-4.69	-3.9	-6.7
	RMSE (mg/L)	14.2	14.3	14.4	13.94	13.69	14.8
	r	0.6	0.6	0.6	0.59	0.59	0.61
Changwu	ME (mg/L)	0.88	1.18	-0.58	-0.9	-4.2	-12.5
	RMSE (mg/L)	6.92	6.98	7.87	10.4	12.2	17.8
	r	0.84	0.84	0.84	0.68	0.69	0.70
An'sai	ME (mg/L)	1.59	1.52	0.62	1.01	1.21	0.77
	RMSE (mg/L)	2.86	2.77	3.8	3.16	3.12	3.21
	r	0.62	0.6	0.58	0.54	0.56	0.51
Shenmu	ME (mg/L)	0.52	0.91	0.85	-3.70	-3.17	-3.19
	RMSE (mg/L)	1.21	1.4	1.5	4.13	3.78	3.53
	r	0.78	0.79	0.7	0.73	0.74	0.71

5 Future predictions of the arrival time of nitrate at the water table

As was shown in previous studies, and illustrated here again, the total storage of nitrate in the deep vadose zone can be inferred from simple mass balance approaches (Botros et al., 2012; Akbariyeh et al., 2018). However, the differences between the loess representation in the simple piston model and more complex numerical modeling approaches have implications regarding nitrate arrival to groundwater. Future simulations were run to predict the nitrate breakthrough curves (BTCs) at the water table using the four modeling approaches (Figure 10). The atmospheric inputs for the future scenarios were the calculated monthly mean values of rain, ET_c and air temperatures of the meteorological data, which were distributed equally at a daily time step. Only at the An'sai site, there is a future yearly nitrate input. Note that the predicted BTCs at Yangling and Changwu sites show similar time scales, where the first arrival of the nitrate at the water table is predicted to occur in the next 30 to 60 years (Figure 10a,b). At Shenmu, the nitrate breakthrough is predicted after about 1000 years (Figure 10c). Various nitrate first arrival times at the water table were predicted for the An'sai site, ranging between thousands and hundreds of thousands of years (Figure 10d). Except for the An'sai site, which is an active farming site, the predicted nitrate concentrations at the water table do not exceed drinking-water standards of the World Health Organization (WHO, 2016). However, in active rainfed and irrigated agriculture areas in the south of the loess plateau similar to the Yangling and Changwu sites (Figure 1), the nitrate concentrations that will arrive to water table are expected to be higher (Turkeltaub et al., 2018). The predicted nitrate arrival times agree with previous plot and regional investigations (Huang 2013; Turkeltaub et al., 2018; Liu et al., 2019; Ji et al., 2019).

Using the HOM, EXP and HET models to predict the first arrival of nitrate to water table indicate similar nitrate arrival times for the Yangling site (Figure 10a). In Changwu, the EXP model predicts earlier nitrate arrival compared with the HOM and HET models (Figure 10b). At the Shenmu site, the EXP and HOM models show similar arrival times, where the nitrate arrivals according to the HET model occurs later (Figure 10d). Large differences between predicted nitrate arrival are displayed for the An'sai site (Figure 10c). Note that the vadose zone at the An'sai site is substantially thicker (141 m depth) compared to the other sites, which partly explains the large time scales of the nitrate first appearance at the water table. Furthermore, it seems that the loess vertical variability might have a long-term effect on nitrate transport in the vadose zone. The differences in the simulated nitrate arrival times and concentrations using the HOM, EXP and HET models are a function of the water velocities, which are affected by the vertical variability of the hydraulic functions. Furthermore, the alternation in water velocities has a linear effect on the dispersion of nitrate, which is directly reflected in the spreading of the nitrate BTCs. This influence was not expressed during the calibration process presented in the current study since most of the nitrate is accumulated in the top third of the loess vadose zone. The results in Figure 10 indicate a joint influence of vadose zone thickness and vertical variability on nitrate transport in the loess vadose zone. To improve our understanding of which site is likely to show sensitivity to the vertical variability, a time series of nitrate measurements is needed. Furthermore, recently it has been shown that the soil water balance in the LPC might be affected by climate change, especially due to possible changes in rain variability (Li et al., 2021). Note that the possible effect of climate change on solute transport was not accounted for in the current study and should be further elaborated.

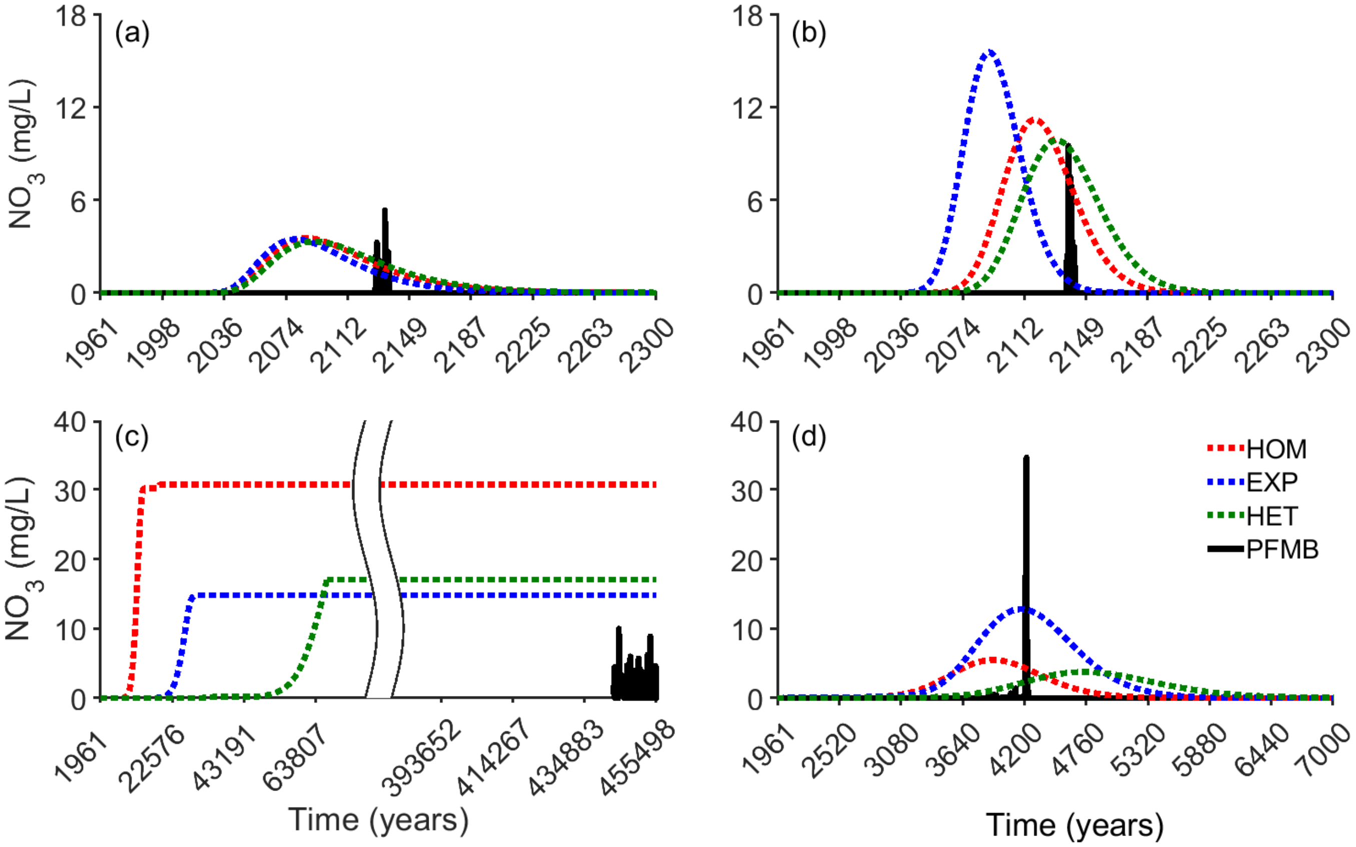

Figure 10. *Predicted time series of nitrate concentration arriving at the water table for (a) Yangling (b) Changwu, (c) An'sai and (d) Shenmu. The (a) Yangling and (b) Changwu sites have the same x (time) and y (nitrate concentration) coordinates. The (c) An'sai and (d) Shenmu sites have the same y (nitrate concentration) coordinates but different x (time) coordinates. A broken x axis in (c) An'sai indicates truncation in time since the predictions of the nitrate time series under this site extend over thousands of years.*

It appears that the PFMB approach substantially overestimates the time of first arrival of nitrate at the water table for all sites (Figure 10). Furthermore, the piston flow approach explicitly implies that the nitrate arrives as one concentrated cluster, while the numerical models account for nitrate arrival that is spread over time (Figure 10). For sites that are characterized with high nitrate concentrations, the contribution of nitrate to groundwater might extend over long periods of time. Knowledge regarding the time scales of the nitrate BTC might determine the approaches of handling the nitrate contamination such as groundwater treatment or shutting down wells. The dilemma of which model is best to implement for unsaturated water flow and nitrate transport was discussed recently by Turkeltaub et al. (2020) from a regional perspective. They compared regional scale simulated nitrate storage and travel times in the vadose zone that were calculated by a piston flow and nitrate mass balance approach (in a global model) and by numerical models (regional model). It was shown that the global model overestimated travel times of nitrate in the loess vadose zone as it is described in the current study. The implementation of a one-layer Richards' equation and ADE appears to be a better modeling tool for the investigation of nitrate migration in the vadose zones of the Chinese Loess Plateau.

Throughout the calibration process, a comparison between simulated and observed nitrate and water content profiles illustrated that including the *Ks* decay function (EXP model) in the numerical models improve the performance of model simulations. Thus, nitrate arrival times at the water table that were predicted by the EXP model are more reliable. The advantage of the *Ks* decay function is that it can be established by using surrogate data such as bulk densities and particle size distributions. Therefore, the Ks decay can be relatively easily inferred for local scale studies and according to global scale data repositories of soil properties (e.g. Hengl et al., 2017). Ultimately, the Richards equation and ADE driven by site-specific general knowledge and basic representation of vertical spatial variability of the hydraulic properties provide a remarkably good representation of nitrate in deep vadose zones, even prior to calibration. Hence, it may be a reasonable forecasting tool at unmeasured sites and may be useful for integration in decision support tools for land management.

6 Conclusions

Models of different complexity were implemented to describe the nitrate transport in four deep loess vadose zones of the Chinese Loess Plateau. A piston flow and nitrate mass-balance (PFMB) approach was implemented to simulate nitrate storage and vertical transport in the loess vadose zone. Simulation results indicate that assuming advective transport only provides a good approximation of nitrate storage, but overestimates nitrate travel times in the loess vadose zone and the nitrate first arrival at the water table. To improve the description of the dispersion process and to include loess variability, a one layer Richards' equation and the ADE with nitrate reactions was applied. Three different conceptualizations of the numerical models were calibrated against deep vadose zone nitrate and water content observations: (1) one-layer model assuming homogenous loess vadose zone (HOM), (2) a model that comprises the Ks decay function (EXP) and (3) a model where the Miller-Miller factors are prescribed to account for changes of water retention and the hydraulic conductivity functions with depth (HET). Accounting for the vertical Ks decay (EXP model) in the numerical models improved the model performance for water flow. It appears that the vertical variability in loess vadose zone might have a long-term effect on nitrate arrival times to water table. However, one aspect that was not included in the current study is the vertical variability of the λ parameter. Most studies in vadose zone environments prescribe one value for λ according to the length of the simulated column. There is lack of knowledge regarding the appropriate scaling approach that should be implemented to account for λ vertical variability in vadose zone modeling.

This study is only based on four sites in the Loess Plateau of China, which limits the straightforward application of the study's outcomes to other loess sites or to larger scales. Nevertheless, the presented approach can be used in locations where only elements of the dataset are available, such as climate data, topsoil properties and history of cultivation. Moreover, the current study has evaluated the effect of vertical variability in the loess deep vadose zone on nitrate transport, which has been rarely done before. Considering the LPC intensive agriculture development, future research should focus on the different hydrological aspects that facilitate nitrate transport in the loess vadose zone. For example, examining the temporal changes in nitrate storage and travel times following the alternation of crop type during the year or even permanently (land use change). An additional aspect that should be explored is the spatial relationship between nitrate storage and agriculture land uses.

Acknowledgments

This work was supported by the Natural Environment Research Council (grant NE/N007409/1 and NE/S009159/1 awarded to Lancaster) and the National Natural Science Foundation of China (41571130081). We thank Rhys Ashton for his help in measuring the loess hydraulic curves. The data archiving is underway using the Lancaster University data repository facilities. The data is available for public download through the following link: 10.17635/lancaster/researchdata/322.

References

Akbariyeh, S., Bartelt-Hunt, S., Snow, D., Li, X., Tang, Z., & Li, Y. (2018). Three-dimensional modeling of nitrate-N transport in vadose zone: Roles of soil heterogeneity and groundwater flux. *Journal of contaminant hydrology*, 211, 15-25. https://doi.org/10.1016/j.jconhyd.2018.02.005

Ameli, A. A., Amvrosiadi, N., Grabs, T., Laudon, H., Creed, I. F., McDonnell, J. J., & Bishop, K. (2016). Hillslope permeability architecture controls on subsurface transit time distribution and flow paths. Journal of Hydrology, 543, 17-30. https://doi.org/10.1016/j.jhydrol.2016.04.071

Ascott, M.J., Gooddy, D.C., Wang, L., Stuart, M.E., Lewis, M.A., Ward, R.S., & Binley, A.M. (2017). Global Patterns of Nitrate Storage in the Vadose Zone. *Nature Communication*, 8, 1416. https://doi.org/10.1038/s41467-017-01321-w.

Albertsona, J.D., & Kiely, G. (2001). On the structure of soil moisture time series in the context of land surface models. *Journal of Hydrology*, 243,101–119. https://doi.org/10.1016/S0022-1694(00)00405-4.

Allen, R. G., Pereira, L. S., Raes, D., & Smith, M. (1998). Crop evapotranspiration: Guidelines for computing crop water requirements, FAO Irrigation and Drainage Pap. 56, Food and Agric. Organ of the U. N., Rome.

Baram, S., Couvreur, V., Harter, T., Read, M., Brown, P.H., Kandelous, M., Smart, D.R., & Hopmans, J.W. (2016). Estimating nitrate leaching to groundwater from orchards: comparing crop nitrogen excess, deep vadose zone data-driven estimates, and HYDRUS modeling. *Vadose Zone Journal*, 15(11). https://doi.org/10.2136/vzj2016.07.0061.

Baran, N., Richert, J., & Mouvet, C. (2007). Field data and modelling of water and nitrate movement through deep unsaturated loess. *Journal of Hydrology*, 345, 27–37. https://doi.org/10.1016/j.jhydrol.2007.07.006

Baudena, M., Bevilacqua, I., Canone, D., Ferraris, S., Previati, M., & Provenzale, A. (2012). Soil water dynamics at a midlatitude test site: Field measurements and box modeling approaches. Journal of Hydrology, 414, 329-340. https://doi.org/10.1016/j.jhydrol.2011.11.009.

Bishop, T. F. A., McBratney, A. B., & Laslett, G. M. (1999). Modelling soil attribute depth functions with equal-area quadratic smoothing splines. Geoderma, 91(1-2), 27-45. https://doi.org/10.1016/S0016-7061(99)00003-8.

Beven, K. J., & Kirkby, M. J. (1979). A physically based, variable contributing area model of basin hydrology/Un modèle à base physique de zone d'appel variable de l'hydrologie du bassin versant. Hydrological Sciences Journal, 24(1), 43-69.

Botros, F. E., Onsoy, Y. S., Ginn, T. R., & Harter, T. (2012). Richards equation–based modeling to estimate flow and nitrate transport in a deep alluvial vadose zone. *Vadose Zone Journal*, 11(4). https://doi.org/10.2136/vzj2011.0145.

Canadell J., R.B. Jackson, J.R. Ehleringer, H.A. Mooney, O.E. Sala, & Schulze, E. D. (1996). Maximum rooting depth of vegetation types at the global scale. *Oecologia*, 108, 583– 595.

Catt, J. A. 2001. The agricultural importance of loess. *Earth-Science Reviews*, 54, 213-229. https://doi.org/10.1016/S0012-8252(01)00049-6.

Clausnitzer, V., Hopmans, J. W. & Nielsen D. R. (1992). Simultaneous scaling of soil water retention and hydraulic conductivity curves. *Water Resources Research*, 28, 19–31. https://doi.org/10.1029/91WR02224.

Clausnitzer, V., & Hopmans, J.W. (1995). Non-linear parameter estimation: LM2OPT. General-purpose optimization code based on the Levenberg–Marquardt algorithm. Land, Air and Water Resour. Pap. no. 100032. University of California, Davis.

Derbyshire, E., Wang, J.T., Billard, A., Egels, Y., Jones, D.K.C.,Kasser, M., Muxart, T., Owen, L., 1991. Landslides in theGansu loess of China. In: Okuda, S., Rapp, A., Zhang, L.Ž.Eds. , Loess: Geomorphological Hazards and Processes. Catena Suppl., vol. 20, pp. 119–145.

Derbyshire, E., Kemp, R. A., & Meng, X. (1997). Climate change, loess and palaeosols: proxy measures and resolution in North China. Journal of the Geological Society, 154(5), 793-805. https://doi.org/10.1144/gsjgs.154.5.0793

Derbyshire, E. (2001). Geological hazards in loess terrain, with particular reference to the loess regions of China. Earth-Science Reviews, 54(1-3), 231-260. https://doi.org/10.1016/S0012-8252(01)00050-2

el Etreiby, F., & Laudelout, H. (1988). Movement of nitrite through a loess soil. Journal of Hydrology, 97, 213–224. https://doi.org/10.1016/0022-1694(88)90116-3.

Fan, T., Stewart, B. A., Yong, W., Junjie, L., & Guangye, Z. (2005). Long-term fertilization effects on grain yield, water-use efficiency and soil fertility in the dryland of Loess Plateau in China. *Agriculture, Ecosystems & Environment*, 106, 313–329. https://doi.org/10.1016/j.agee.2004.09.003

Fan, Y., Li, H., & Miguez-Macho, G. (2013). Global patterns of groundwater table depth. *Science*, 339(6122), 940–943.

Fan, J., Wang, Q., Jones S. B., & Shao M. (2016). Soil water depletion and recharge under different land cover in China's Loess Plateau. *Ecohydrology*., 9, 396–406. https://doi.org/10.1002/eco.1642.

Feyen, J., Jacques, D., Timmerman, A., & Vanderborght, J. (1998). Modelling water flow and solute transport in heterogeneous soils: A review of recent approaches. *Journal of Agricultural Engineering Research*, 70(3), 231-256. https://doi.org/10.1006/jaer.1998.0272.

Feddes, R.A., Kowalik, P.J., & Zaradny, H. (1978). Simulation of field water use and crop yield. John Wiley and Sons, New York.

Galloway, J. N., Dentener, F. J., Capone, D. G., Boyer, E. W., Howarth, R. W., Seitzinger, S. P., Asner, G. P., Cleveland, C. C., Green, P. A., Holland, E. A., Karl, D. M., Michaels, A. F., Porter, J. H., Townsend, A. R., & Vöosmarty, C. J. (2004). Nitrogen cycles: past, present, and future. *Biogeochemistry* 70, 153–226. https://doi.org/10.1007/s10533-004-0370-0.

Gates, J. B., Scanlon, B. R., Mu, X., & Zhang, L. (2011). Impacts of soil conservation on groundwater recharge in the semi-arid Loess Plateau, China. Hydrogeology Journal, 19, 865. https://doi.org/10.1007/s10040-011-0716-3

Green, C. T., Fisher, L. H., & Bekins, B.A. (2008). Nitrogen fluxes through unsaturated zones in five agricultural settings across the United States. *Journal of Environmental Quality*, 37, 1073–1085. doi.org/10.2134/jeq2007.0010.

Guswa, A. J., Celia, M. A., & Rodriguez-Iturbe, I. (2002). Models of soil moisture dynamics in ecohydrology: A comparative study. Water Resources Research, 38(9), 5-1. https://doi.org/10.1029/2001WR000826.

Hanson, B. R., Šimůnek, J., & Hopmans, J. W. (2006). Evaluation of urea-ammonium-nitrate fertigation with drip irrigation using numerical modeling. *Agriculture Water Management*, 86, 102–113. https://doi.org/10.1016/j.agwat.2006.06.013.

Hengl, T., Mendes de Jesus, J., Heuvelink, G. B., Ruiperez Gonzalez, M., Kilibarda, M., Blagotić, A., ... & Guevara, M. A. (2017). SoilGrids250m: Global gridded soil information based on machine learning. PLoS one, 12(2), e0169748. https://doi.org/10.1371/journal.pone.0169748.

Hillel, D. 1998. Environmental soil physics. 1st ed. Academic Press, Elsevier, New York.

Huang, M., Gallichand, J., & Zhong, L. (2004). Water–yield relationships and optimal water management for winter wheat in the Loess Plateau of China. *Irrigation Science*, 23, 47–54. https://doi.org/10.1007/s00271-004-0092-z.

Huang, T., & Pang, Z. (2011). Estimating groundwater recharge following land-use change using chloride mass balance of soil profiles: A case study at Guyuan and Xifeng in the Loess Plateau of China. *Hydrogeology Journal*, 19, 177 186. https://doi.org/10.1007/s10040-010-0643-8

Huang, T., Pang, Z., & Yuan, L. (2013). Nitrate in groundwater and the unsaturated zone in (semi) arid northern China: Baseline and factors controlling its transport and fate. *Environment and Earth Science*, 70, 145–156. https://doi.org/10.1007/s12665-012-2111-3

Kabat, P. R. W. A., Hutjes, R. W. A., & Feddes, R. A. (1997). The scaling characteristics of soil parameters: From plot scale heterogeneity to subgrid parameterization. *Journal of Hydrology*, 190(3-4), 363-396. https://doi.org/10.1016/S0022-1694(96)03134-4.

Kang, S., Gu, B., Du, T., & Zhang, J. (2003). Crop coefficient and ratio of transpiration to evapotranspiration of winter wheat and maize in a semi-humid region. *Agriculture Water Management*, 59, 239-254. https://doi.org/10.1016/S0378-3774(02)00150-6.

Kapoor, A. & Viraraghavan, T. Nitrate removal from drinking water-review. *Journal of Environmental Engineering*, 123, 371–380 (1997). https://doi.org/10.1061/(ASCE)0733-9372(1997)123:4(371).

Keller, C.K., Butcher, C.N., Smith, J.L., & Allen-King, R.M. (2008). Nitrate in tile drainage of the semiarid Palouse basin. *Journal of Environmental Quality*, 37, 353-361. https://doi.org/10.2134/jeq2006.0515.

Kukla, G.J. (1987). Loess stratigraphy in Central China. *Quaternary Science Reviews*, 6, 191-207. https://doi.org/10.1029/2004WR003841.

Kurtzman, D., Shapira, R. H., Bar-Tal, A., Fine, P., and Russo, D. (2013). Nitrate fluxes to groundwater under citrus orchards in a Mediterranean climate: Observations, calibrated models, simulations and agro-hydrological conclusions. *Journal of Contaminant Hydrology*, 151, 93–104. https://doi.org/10.1016/j.jconhyd.2013.05.004.

Isla, F.I., Londoño, O.M.Q., & Cortizo, L.C. (2018). Groundwater characteristics within loessic deposits: the coastal springs of Los Acantilados, Mar del Plata, Argentina. *Environmental Earth Sciences*, 77, 610. https://doi.org/10.1007/s12665-018-7766-y.

Izbicki, J.A., Radyk, J., & Michel, R.L. (2000). Water movement through a thick unsaturated zone underlying an international stream in the western Mojave Desert, southern California, USA. *Journal of Hydrology*, 238, 194–217. https://doi.org/10.1016/S0022-1694(00)00331-0.

Jansson, P., Anderson, R., 1988. Simulation of runoff and nitrate leaching from an agricultural district in Sweden. J. Hydrol. 99, 33–47. https://doi.org/10.1016/0022-1694(88)90076-5.

Ji, W., Huang, Y., Li, B., Hopkins, D. W., Liu, W., & Li, Z. (2020). Legacy nitrate in the deep loess deposits after conversion of arable farmland to non-fertilized land uses for degraded land restoration. *Land Degradation & Development*, 31(11), 1355-1365. https://doi.org/10.1002/ldr.3532.

Jiang, X. W., Wan, L., Wang, X. S., Ge, S., and Liu J. (2009). Effect of exponential decay in hydraulic conductivity with depth on regional ground-water flow. *Geophysical Research Letters* ,36, L24402. https://doi.org/10.1029/2009GL041251.

Jia, X., Shao, M. A., Zhang, C., & Zhao, C. (2015). Regional temporal persistence of dried soil layer along south–north transect of the Loess Plateau, China. *Journal of Hydrology*, 528, 152–160. https://doi.org/10.1016/j.jhydrol.2015.06.025.

Jia, X., Zhu, Y., Huang, L., Wei, X., Fang, Y., Wu, L., Binley, A., & Shao, M. (2018). Mineral N stock and nitrate accumulation in the 50 to 200 m profile on the Loess Plateau. *Science of the Total Environment,* 633, 999-1006. https://doi.org/10.1016/j.scitotenv.2018.03.249.

Laio, F., Porporato, A., Ridolfi, L., & Rodriguez-Iturbe, I. (2001). Plants in water-controlled ecosystems: active role in hydrologic processes and response to water stress: II. Probabilistic soil moisture dynamics. Advances in water resources, 24(7), 707-723. https://doi.org/10.1016/S0309-1708(01)00005-7.

Leenhardt, D., Lafolie, F., & Bruckler, L. (1998). Evaluating irrigation strategies for lettuce by simulation: 1. Water flow simulations. *European Journal of Agronomy*, 8, 249–265. https://doi.org/10.1016/S1161-0301(97)00065-8

Li, C., Qi, J., Wang, S., Yang, L., Yang, W., & Zou, S. (2014). A holistic system approach to understanding underground water dynamics in the Loess Tableland: A case study of the Dongzhi Loess Tableland in Northwest China. *Water Resources Management*, 28, 2937–2951. https://doi.org/10.1007/s11269-014-0647-6

Li, B., Biswas, A., Wang Y., & Li, Z. (2021). Identifying the dominant effects of climate and land use change on soil water balance in deep loessial vadose zone. *Agricultural Water Management*, 245, 106637. https://doi.org/10.1016/j.agwat.2020.106637

Li, Y., Šimůnek, J., Zhangb, Z., Jing, L., & Nia, L. (2015). Evaluation of nitrogen balance in a direct-seeded-rice field experiment using Hydrus-1D. *Agriculture Water Management*, 148, 213–222. https://doi.org/10.1016/j.agwat.2014.10.010.

Liu, Z., Ma, P., Zhai, B., & Zhou, J. (2019). Soil moisture decline and residual nitrate accumulation after converting cropland to apple orchard in a semiarid region: Evidence from the Loess Plateau. *Catena*, 181, 104080. https://doi.org/10.1016/j.catena.2019.104080.

Miller, E.E. & Miller, R.D. (1956). Physical theory for capillary flow phenomena. *Journal of Applied Physics*, 27, 324–332. https://doi.org/10.1063/1.1722370.

Min, L., Shen, Y., & Pei, H. (2015). Estimating groundwater recharge using deep vadose zone data under typical irrigated cropland in the piedmont region of the North China Plain. *Journal of Hydrology*, 527, 305-315. https://doi.org/10.1016/j.jhydrol.2015.04.064.

Min, L., Shen, Y., Pei, H., & Jing, B. (2017). Characterising deep vadose zone water movement and solute transport under typical irrigated cropland in the North China Plain. *Hydrological Processes*, 31(7), 1498-1509. https://doi.org/10.1002/hyp.11120.

Mohanty, B. P., & J. Zhu (2007), Effective soil hydraulic parameters in horizontally and vertically heterogeneous soils for steady-state land–atmosphere interaction. *Journal of Hydrometeorology*, 8, 715–729. https://doi.org/10.1175/JHM606.1.

Mualem, Y. (1976). A new model for predicting the hydraulic conductivity of unsaturated porous media. *Water Resources Research*, 12, 513–522. https://doi.org/10.1029/WR012i003p00513.

Nasta, P., & Romano, N. (2016). Use of a flux-based field capacity criterion to identify effective hydraulic parameters of layered soil profiles subjected to synthetic drainage experiments. *Water Resources Research*, 52, 566-584. https://doi.org/10.1002/2015WR016979.

Nimmo, J. R., Deason, J. A., Izbicki, J. A., & Martin, P. (2002). Evaluation of unsaturated zone water fluxes in heterogeneous alluvium at a Mojave Basin site. *Water Resources Research*, 38(10), 33-1. https://doi.org/10.1029/2001WR000735.

O'Geen, A. T., McDaniel, P. A., Boll, J., & Keller, C. K. (2005). Paleosols as deep regolith: Implications for ground-water recharge across a loessial climosequence. *Geoderma*, 126(1-2), 85-99. https://doi.org/10.1016/j.geoderma.2004.11.008.

Onsoy, Y. S., Harter, T., Ginn, T. R., & Horwath, W. R. (2005). Spatial variability and transport of nitrate in a deep alluvial vadose zone. *Vadose Zone Journal*, 4, 41–54. https://doi.org/10.2136/vzj2005.0041.

Oostrom, M., Truex, M.J., Last, G.V., Strickland, C.E. & Tartakovsky, G.D. (2016). Evaluation of deep vadose zone contaminant flux into groundwater: Approach and case study. *Journal of contaminant hydrology*, 189, 27-43. https://doi.org/10.1016/j.jconhyd.2016.03.002.

Porporato, A., D'odorico, P., Laio, F., & Rodriguez-Iturbe, I. (2003). Hydrologic controls on soil carbon and nitrogen cycles. I. Modeling scheme. Advances in water resources, 26(1), 45-58. https://doi.org/10.1016/S0309-1708(02)00094-5.

Ramos, T. B., Šimůnek, J., Gonçalves, M. C., Martins, J. C., Prazeres, A., Castanheira, N. L., & Pereira, L. S. (2011). Field evaluation of a multicomponent solute transport model in soils irrigated with saline waters. *Journal of Hydrology*, 407, 129–144. https://doi.org/10.1016/j.jhydrol.2011.07.016

Ritchie, J. T., Model for predicting evaporation from a row crop with incomplete cover, *Water Resources Research*, 8(5), 1204-1213, 1972. https://doi.org/10.1029/WR008i005p01204.

Rochette, P., Angers, D. A., Chantigny, M. H., Gasser, M. O., MacDonald, J. D., Pelster, D. E., & Bertrand, N. (2014). Ammonia volatilization and nitrogen retention: How deep to incorporate urea? *Journal of Environmental Quality*, 42, 1635–1642. https://doi.org/10.2134/jeq2013.05.0192

Romano, N., Palladino, M., & Chirico, G. B. (2011). Parameterization of a bucket model for soil-vegetation-atmosphere modeling under seasonal climatic regimes. Hydrology & Earth System Sciences, 15(12). https://doi.org/10.5194/hess-15-3877-2011

Russo, D., Laufer, A., Gerstl, Z., Ronen, D., Weisbrod, N., & Zentner, E. (2014). On the mechanism of field-scale solute transport: Insights from numerical simulations and field observations. Water Resources Research, 50(9), 7484-7504. https://doi.org/10.1002/2014WR015514.

Sadeghi, M., Ghahraman, B., Warrick, A. W., Tuller, M., & Jones, S. B. (2016). A critical evaluation of the Miller and Miller similar media theory for application to natural soils. *Water Resources Research*, 52(5), 3829-3846.

Schwen, A., Zimmermann, M., & Bodner, G. (2015). Vertical variations of soil hydraulic properties within two soil profiles and its relevance for soil water simulations. *Journal of hydrology*, 516, 169-181.

Šimůnek, J., Šejna, M., Saito, H., Sakai, M., & van Genuchten, M.Th. (2008). The HYDRUS-1D Software Package for Simulating the Movement of Water, Heat, and Multiple Solutes in Variably Saturated Media. Version 4.0. HYDRUS Software Series 3. Dep. Environmental Sciences, Univ. Calif. Riverside, Riverside, CA.

Smalley, I., Marković, S. B., & Svirčev, Z. (2011). Loess is [almost totally formed by] the accumulation of dust. *Quaternary International*, 240, 4-11. https://doi.org/10.1016/j.quaint.2010.07.011.

Smalley, I.J., & Marković, S.B. (2014). Loessification and hydroconsolidation: there is a connection. *Catena*, 117, 94-99. https://doi.org/10.1016/j.catena.2013.07.006.

Spalding, R.F., & Exner, M.E. (1993). Occurrence of nitrate in groundwater — a review. *Journal of Environmental Quality*, 22, 392-402. https://doi.org/10.2134/jeq1993.00472425002200030002x

van Genuchten, M. T. (1980). A closed-form equation for predicting the hydraulic conductivity of unsaturated soils. *Soil Science Society of America Journal*, 44, 892–898.

Turkeltaub, T., Dahan, O., & Kurtzman, D. (2014). Investigation of groundwater recharge under agricultural fields using transient deep vadose zone data. *Vadose Zone Journal*, 13(4). https://doi.org/10.2136/vzj2013.10.0176

Turkeltaub, T., Kurtzman, D., Bel, G., & Dahan, O. (2015a). Examination of groundwater recharge with a calibrated/validated flow model of the deep vadose zone. *Journal of Hydrology*, 522, 618-627. https://doi.org/10.1016/j.jhydrol.2015.01.026.

Turkeltaub, T., Kurtzman, D., Russak, E. E., & Dahan, O. (2015b). Impact of switching crop type on water and solute fluxes in deep vadose zone. *Water Resources Research*, 51(12), 9828-9842. https://doi.org/10.1002/2015WR017612.

Turkeltaub, T., Jia, X., Zhu, Y., Shao, M. A., & Binley, A. (2018). Recharge and Nitrate Transport Through the Deep Vadose Zone of the Loess Plateau: A Regional-Scale Model

Investigation. *Water Resources Research*, 54(7), 4332-4346. https://doi.org/10.1029/2017WR022190.

Turkeltaub, T., Ascott, M. J., Gooddy, D. C., Jia, X., Shao, M. A., & Binley, A. (2020). Prediction of regional-scale groundwater recharge and nitrate storage in the vadose zone: A comparison between a global model and a regional model. *Hydrological Processes*, 34(15), 3347-3357. https://doi.org/10.1002/hyp.13834.

Vanderborght, J., & Vereecken, H. (2007). Review of dispersivities for transport modeling in soils. *Vadose Zone Journal*, 6(1), 29-52.

Vereecken, H., Kasteel, R., Vanderborght, J., & Harter, T. (2007). Upscaling hydraulic properties and soil water flow processes in heterogeneous soils. *Vadose Zone Journal*, 6(1), 1-28. https://doi.org/10.2136/vzj2006.0055

Vrugt, J. A., Van Wijk, M. T., Hopmans, J. W., & Simunek, J. (2001). One-, two-, and three-dimensional root water uptake functions for transient modeling. *Water Resources Research*, 37, 2457–2470. https://doi.org/10.1029/2000WR000027.

Wagner, R.J., & Roberts, L.M. (1998). Pesticides and volatile organic compounds in surface and ground water of the Palouse subunit, Central Columbia Plateau, Washington and Idaho, 1993–95. U.S. Geol. Surv. 97, 4285.

Wang, Y., Shao, M. A., & Liu, Z. (2013a). Vertical distribution and influencing factors of soil water content within 21-m profile on the Chinese Loess Plateau. *Geoderma*, 193, 300-310. https://doi.org/10.1016/j.geoderma.2012.10.011.

Wang, Y., Shao, M. A., Liu, Z., & Horton, R. (2013b). Regional-scale variation and distribution patterns of soil saturated hydraulic conductivities in surface and subsurface layers in the loessial soils of China. *Journal of Hydrology*, 487, 13-23. https://doi.org/10.1016/j.jhydrol.2013.02.006.

Wang, W., Wang, Y., Suna, Q., Zhanga, M., Qianga, Y., & Liua, M. (2017). Spatial variation of saturated hydraulic conductivity of a loess slope in the South Jingyang Plateau, China. *Engineering Geology*, 236, 70–78. https://doi.org/10.1016/j.enggeo.2017.08.002

WHO (2016). Nitrate and Nitrite in Drinking-water. Background document for development of WHO Guidelines for Drinking-water Quality , World Health Organization. https://www.who.int/water_sanitation_health/dwq/chemicals/nitrate-nitrite-background-jan17.pdf.

Zhang, X., Zhang, L., Zhao, J., Rustomji, P., & Hairsine, P. (2008). Responses of streamflow to changes in climate and land use/cover in the Loess Plateau, China. *Water Resources Research*, 44, W00A07. https://doi.org/10.1029/2007WR006711

Zhang, Z. F., Ward, A. L., & Gee, G. W. (2004). A combined parameter scaling and inverse technique to upscale the unsaturated hydraulic parameters for heterogeneous soils. *Water resources research*, 40(8). https://doi.org/10.1029/2003WR002925

Zhang, Y., & Schaap, M. G. (2017). Weighted recalibration of the Rosetta pedotransfer model with improved estimates of hydraulic parameter distributions and summary statistics (Rosetta3). *Journal of Hydrology*, 547, 39-53. https://doi.org/10.1016/j.jhydrol.2017.01.004